Applied Catalysis B: Environmental 115–116 (2012) 253–260

Contents lists available at SciVerse ScienceDirect

Applied Catalysis B: Environmental

journal homepage: www.elsevier.com/locate/apcatb

Improving the visible light photocatalytic activity of nano-sized titanium dioxide via the synergistic effects between sulfur doping and sulfation

Yuxiao Niu, Mingyang Xing, Baozhu Tian, Jinlong Zhang*

Key Laboratory for Advanced Materials and Institute of Fine Chemicals, East China University of Science and Technology, 130 Meilong Road, Shanghai 200237, PR China

ARTICLE INFO

Article history:
Received 7 November 2011
Received in revised form
22 December 2011
Accepted 23 December 2011
Available online 31 December 2011

Keywords:
Potassium persulfate
Synergistic action
Sulfur doping
SO_4^{2-}
Phenol degradation

ABSTRACT

S-doped and sulfated nano-sized TiO_2 photocatalysts were prepared by a low-temperature solvothermal method, using potassium persulfate as sulfur source. The obtained samples were characterized by XRD, UV–vis DRS, FTIR, FTIR-pyridine, XPS, and nitrogen adsorption–desorption methods. Compared with undoped TiO_2, the S-doped and sulfated TiO_2 photocatalysts exhibited much higher photocatalytic activity for phenol degradation under visible light irradiation. It was revealed that S was not only incorporated into the crystal lattice of TiO_2 replacing Ti^{4+} (as S^{4+}) but also anchored on its surface in the form of SO_4^{2-}. Further study indicated that there are synergistic effects between doped S and anchored SO_4^{2-} on improving the visible light photocatalytic activity of TiO_2. The doped S can form an impurity level below the conduction band of TiO_2, extending the light response of TiO_2 into visible light region, while SO_4^{2-} anchored on TiO_2 surface is favorable for trapping photo-induced electrons, suppressing the recombination of electrons and holes and consequently promoting the formation of hydroxyl radical.

1. Introduction

Nano-sized TiO_2 photocatalyst has received a great deal of attention since the discovery of the photocatalytic water-splitting on titania electrodes in 1972 [1]. TiO_2 has a promising prospect in many fields, for example, pigments, oxygen sensors and environmental purification. It has been extensively studied as a photocatalyst in water and air cleanup, owing to its high photocatalytic activity, long-term chemical stability, low production costs, and nontoxicity. However, TiO_2 photocatalyst can only be excited with UV light because of its wide band gap (3.2–3.4 eV), which limits the use of the solar energy. Many methods have been used to modify TiO_2 to make its absorption red shift. One alternative approach achieving above the effect is to dope TiO_2 with either nonmetal or metal. For example, nonmetal doping with S [2–5], N [6,7], C [8,9], B [10–12], I [13–15], P [16], F [17,18] was mostly used for the photocatalytic applications in the visible region. For the sulfur doping TiO_2, many groups have found that it has high photoactivity.

Umebayashi et al. [2] synthesized S-doped TiO_2 by oxidation annealing of TiS_2 in which S atoms replaced O atoms (anionic doping) and the S-doped TiO_2 showed a significant red-shift of the absorption edge. Later, Ohno et al. [3] prepared S cation-doped TiO_2 by sol–gel method, in which S atoms substituted for Ti. The photocatalysts had high photoactivity for MB degradation in the visible region. Yu et al. [19] obtained S-doped TiO_2 photocatalysts by hydrothermal treatment of TiS_2 powder in HCl solution at 180 °C, the catalysts having an excellent activity for 4-chlorophenol degradation. In the previous reports, sulfur sources used were TiS_2 [2], thiourea [4,19,20], CS_2 [5], sulfuric acid [21], and Na_2SO_4 [22], in which thiourea was used more widely. S-doped TiO_2 photocatalysts have mainly been prepared by calcining amorphous titania or hydrothermal treatment at high reaction temperatures.

In the present work, we have prepared S-doped TiO_2 photocatalysts by a facile low-temperature solvothermal method, using potassium persulfate ($K_2S_2O_8$) as sulfur source, the surface of which are full of sulfate ions. These sulfate TiO_2 are a kind of solid superacids, which are applicable to various acid catalytic reactions such as isomerization [23], cracking alkylation [24], esterification [25] and photocatalyst [26,27]. It has been proposed that the strong acid property is related to sulfate ions, in which high electron negativity of sulfur can induce polarization of neighboring OH groups [28]. Moreover, the highly polarized state of surface acidity is favorable for trapping photo-induced electrons, resulting in an improved quantum yield with production of reactive hydroxyl group radicals. In the present work, S-doped and sulfated nano-sized TiO_2 photocatalysts were prepared by a low-temperature solvothermal method, using potassium persulfate as sulfur source. Meanwhile, this synthesis method is not only energy efficient, but also environmentally conscious. The nanoparticles prepared by this method were characterized by X-ray powder diffraction (XRD), Fourier transform (FTIR) and FTIR-pyridine, UV–vis

* Corresponding author. Tel.: +86 21 64252062; fax: +86 21 64252062.
E-mail address: jlzhang@ecust.edu.cn (J. Zhang).

0926-3373/$ – see front matter © 2012 Elsevier B.V. All rights reserved.
doi:10.1016/j.apcatb.2011.12.039

diffused reflectance spectra (DRS), X-ray photoelectron spectroscopy (XPS), and Brunauer–Emmett–Teller (BET)-surface areas. The photocatalytic activities of the samples were investigated by the measurement of the phenol degradation in the aqueous suspensions in the visible light region. For the S-doped and sulfated TiO_2 photocatalysts, the high photoactivity may be resulted from the synergistic effect of sulfur doping and the sulfation.

2. Experimental

2.1. Photocatalyst preparation

The S-doped and sulfate TiO_2 photocatalysts were prepared by a low-temperature solvothermal method with potassium persulfate as sulfur source. The detailed procedures are as follows: 14.69 mmol tetrabutyl titanate (TBOT) was added into the ethanol (25 mL) with continuous stirring for 10 min to obtain solution A. Hydrochloric acid (0.1 mol/L, 2 mL) was mixed with the ethanol (25 mL) with continuous stirring for 10 min to obtain solution B. Solution B was added dropwise to solution A, while the mixture was stirred for 20 min. Then, different amounts of potassium persulfate ($K_2S_2O_8$) were added into the mixture, stirring for 40 min. The resultant mixture was then transferred into a 100 mL Teflon-inner-linear stainless steel autoclave, which was kept under 393 K for 12 h. After this hydrothermal treatment, the precipitate was washed by ethanol and water, dried, and ground to obtain the nanoparticles. The samples prepared by this method were S-doped and sulfation denoted as SST-*x*, where *x* describes the molar ratio of $K_2S_2O_8$ to titanium ($x = 0$, 0.25, 0.5, 1.0, 2.0, 3.0). N-TiO_2 [29] and C-TiO_2 [30] were prepared using the methods which has been reported.

2.2. Catalyst characterization

X-ray diffraction patterns of all samples were collected in the range 10–80° (2θ) using a Rigaku D/MAX 2550 diffractometer (Cu Kα radiation, λ = 1.5406 Å), operated at 40 kV and 100 mA. The crystallite size was estimated by applying the Scherrer equation to the full width at half-maximum (FWHM) of the (1 0 1) peak of anatase, with α-silicon (99.9999%) as a standard for the instrumental line broadening. The UV–vis absorbance spectra were obtained for the dry-pressed disk samples using a Scan UV–vis spectrophotometer (Shimadzu, UV-2450) equipped with an integrating sphere assembly, using $BaSO_4$ as the reflectance sample. The spectra were recorded at room temperature in air within the range 200–800 nm. The instrument employed for XPS studies was a Perkin-Elmer PHI 5000C ESCA system with Al Kα radiation operated at 250 W. The shift of the binding energy due to relative surface charging was corrected using the C 1s level at 284.6 eV as an internal standard. Fourier transform spectra were recorded with KBr disks containing the powder sample with the FTIR spectrometer (Nicolet Magna 550) in the range of 4000–400 cm^{-1}. FTIR-pyridine spectra were obtained from Nicolet-5700 spectrometer. The annealed material was pressed into thin self-supported wafers. They were then placed in a glass Pyrex cell coupled with a vacuum line in order to be evacuated (1×10^{-3} Torr) at 400 °C for 2 h. The adsorption was carried out on the cell at 25 °C by breaking a capillary tube, which contained pyridine. The excess pyridine was desorbed under vacuum from room temperature to 400 °C with 100 °C steps. N_2 adsorption–desorption isotherms were measured at 77 K on a micromeritics tristar II 3020 system from which the surface area (BET method), the pore size (Barrett–Joyner–Halenda (BJH) model), and pore volume were calculated. The photoluminescence (PL) emission spectra of the samples were measured using RF-5301PC spectrofluorophotometer (Shimadzu) with a 150 W Xe lamp as excitation source.

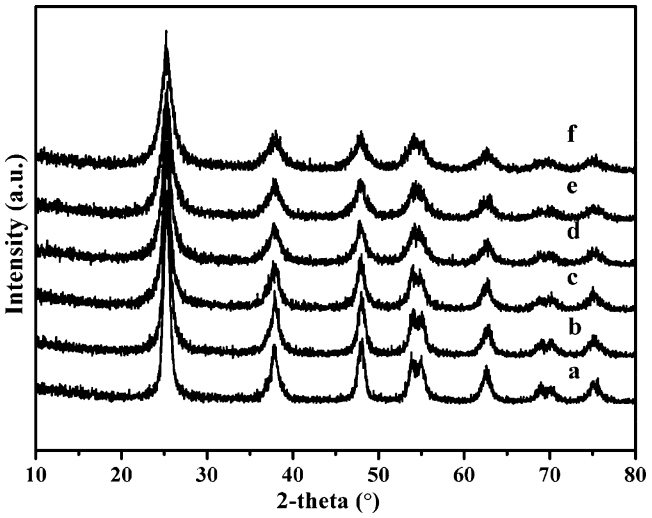

Fig. 1. XRD patterns of the different S-doped and sulfate TiO_2. SST-0 (a), SST-0.25 (b), SST-0.5 (c), SST-1.0 (d), SST-2.0 (e), SST-3.0 (f).

2.3. Photocatalytic measurements

The photocatalytic activity of each sample was evaluated in terms of the degradation of phenol (20 mg/L). The photocatalyst (0.06 g) was added into a 100 mL quartz photoreactor containing 60 mL of 20 mg/L phenol solution. The mixture was stirred for 30 min in the dark to reach the adsorption–desorption equilibrium. A 1000 W tungsten halogen lamp equipped with a UV cutoff filters (λ > 420 nm) was used as a visible light source (the average light intensity was 60 mW cm^{-2}). The lamp was cooled with flowing water in a quartz cylindrical jacket around the lamp, and ambient temperature was maintained during the photocatalytic reaction. At the given time intervals, the analytical samples were taken from the mixture and immediately centrifuged, and then filtered through a 0.22 μm Millipore filter to remove the photocatalysts. The filtrates were analyzed by recording variations in the absorption in UV–vis spectra of phenol using a UV-2450 ultraviolet visible spectrometer.

3. Results and discussion

3.1. X-ray diffraction (XRD)

Fig. 1 gives the XRD patterns of the different SST samples. The diffraction peaks of all samples are ascribed to the TiO_2 anatase phase. These observations indicate that there is virtually no phase change for TiO_2 in the process of sulfur doping, regardless of the amounts of dopants. The crystal sizes of all the samples were estimated using the Scherrer equation:

$$D = \frac{K\lambda}{\beta \cos\theta} \quad (1)$$

where β is the half-height width of the diffraction peak of anatase, $K = 0.89$ is a coefficient, θ is the diffraction angle, and λ is the X-ray wavelength corresponding to the Cu Kα irradiation. As shown in Table 1, the average crystallite size decreases with the increase of S doping amount. The lattice parameters of SST photocatalysts were calculated according to the calculation of the XRD peak (1 0 1) and (1 0 3), and also shown in Table 1. The lattice parameters of different SST photocatalysts have no significant difference in the *a*-axis, however, they are decreasing in the *c*-axis with the increasing sulfur doping, which indicates that sulfur can be doped into TiO_2 crystal lattice. The S substituted for Ti^{4+} hinders the growth of TiO_2, therefore, the particle size of S-doped TiO_2 photocatalysts get smaller with the increasing sulfur doping.

Table 1
Measured structural characteristics of different samples.

	Crystallite size (nm)[a]	Lattice parameters (Å)[a]		Band gap (eV)[b]
		$a = b$	c	
SST-0	13.27	3.79	9.63	2.95
SST-0.25	12.99	3.78	9.59	2.85
SST-0.5	9.41	3.79	9.58	2.83
SST-1.0	7.34	3.79	9.52	2.78
SST-2.0	6.12	3.79	9.47	2.79
SST-3.0	6.73	3.78	9.46	2.82

[a] Calculated according to the XRD results.
[b] Calculated according to the UV–vis DRS results.

3.2. UV–vis diffused reflectance spectra (DRS)

UV–vis diffuse reflectance spectra of SST samples are shown in Fig. 2a. It can be seen that the absorptions of S-doped TiO_2 photocatalysts are enhanced in visible light compared with the undoped TiO_2. This is consistent with the results which Bidaye et al. [31] have reported. The enhanced absorptions of S-doped TiO_2 photocatalysts are in accordance with the changes of the lattice parameters in the *c*-axis of the XRD patterns [32]. Kubelka–Munk function was used to estimate the band gap energy of the prepared samples by plotting $(\alpha h\nu)^{1/2}$ versus energy of light (Fig. 2b). And the band gap energies of SST catalysts are shown in Table 1. The band gap energy of SST-0 catalyst is 2.95 eV, and the band gap energies of S-doped TiO_2 catalysts are 2.78–2.85 eV. The band gap energies of the S-doped TiO_2 are decreased as compared to undoped sample. This can extend the utilization of S-doped TiO_2 to the visible light region.

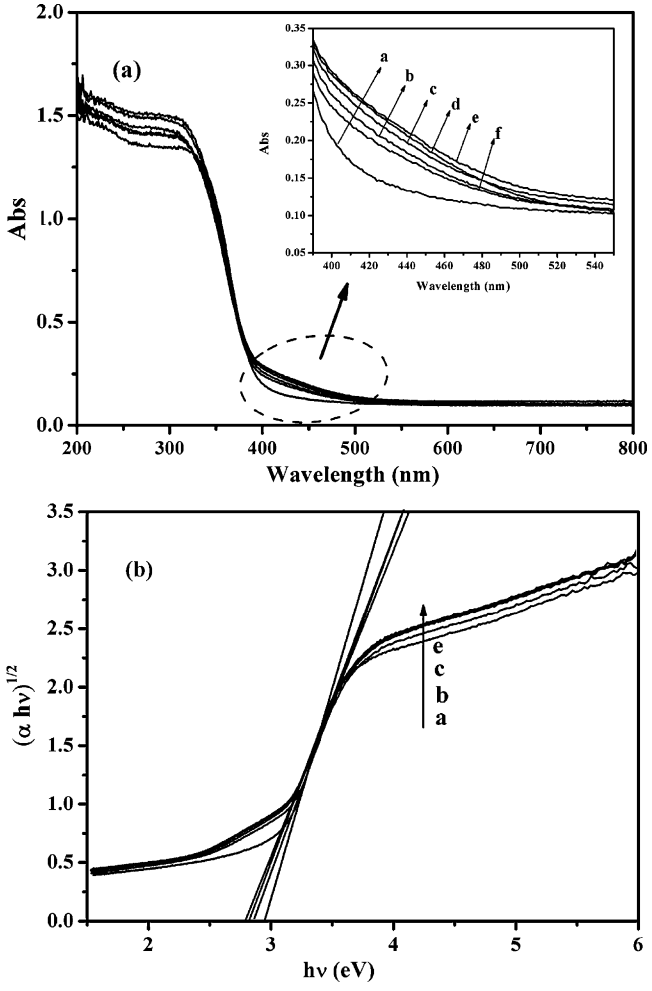

Fig. 2. UV–vis diffuse reflectance spectra of the different S-doped and sulfate TiO_2. SST-0 (a), SST-0.25 (b), SST-0.5 (c), SST-1.0 (d), SST-2.0 (e), SST-3.0 (f).

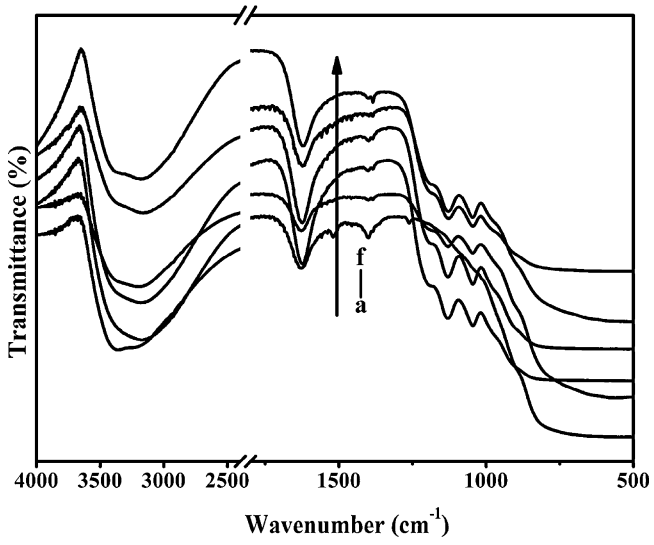

Fig. 3. FTIR spectra of the different S-doped and sulfate TiO_2. SST-0 (a), SST-0.25 (b), SST-0.5 (c), SST-1.0 (d), SST-2.0 (e), SST-3.0 (f).

3.3. FTIR and FTIR-pyridine

The FTIR spectra of different SST samples are shown in Fig. 3. The peaks corresponding to 1643 cm^{-1} and 3300–3500 cm^{-1} can be attributed to H—O—H bending vibration of adsorbed water and the broad absorption band [33], respectively, which indicates the presence of hydroxyl groups on the surface of samples. For the SST-0 catalyst, the absorptions at 1550–1250 cm^{-1} can be assigned to carboxylate asymmetric stretching vibration (1523 cm^{-1}), C—H bending vibration (1400–1380 cm^{-1}) and C—O stretching vibration (1262 cm^{-1}) [34]. This indicates that there is much carbonate species on the surface of the TiO_2 catalyst without sulfur doping. Compared with SST-0 catalyst, all the S-doped samples have similar absorption patterns showing new peaks in the region of 900–1300 cm^{-1} together with the disappearance of the two peaks at 1523 and 1262 cm^{-1}. The peaks located at 1040, 1130 and 1202 cm^{-1} are the characteristic frequencies of sulfate coordinated to metal (such as Ti^{4+}) in bidentate model [35]. The peak at 1040 cm^{-1} is assigned to the S—O stretching frequencies in S—O—Ti and the peaks at 1130 and 1202 cm^{-1} belong to S═O stretching frequencies of bridged bidentate sulfate [36,37]. The introduction of sulfate into TiO_2 result in the sulfates being anchored on the surface of TiO_2, leading to decrease in the carbonate species, hence improving the photocatalytic activity of S-doped and sulfate TiO_2.

The FTIR(pyridine thermodesorption spectra of SST photocatalysts are presented in Fig. 4. The absorbance bands at 1445, 1490, 1575 and 1606 cm^{-1} can be attributed to the Lewis acidic sites, while the absorbance band around 1540 cm^{-1} belongs to the Brönsted acidic sites [38]. According to the spectra, the SST-0 photocatalyst displays Lewis acidic sites, which may be caused by the carbonate species on the surface of TiO_2. With sulfur doping, the SST-0.5 photocatalyst shows Lewis acidic sites and Brönsted acidic sites corresponding to a broad absorbance band around 1540 cm^{-1}. The structure of Ti and SO_4^{2-} bidentate model is shown in Scheme 1. The Brönsted acidic sites may have resulted from the surface SO_4^{2-} species adsorbed on TiO_2 while the Lewis acidic sites could be attributed to the bridged bidentate coordination between SO_4^{2-} and TiO_2. The FTIR-pyridine thermodesorption spectra were recorded under the condition of vacuum drying (400 °C) for 2 h,

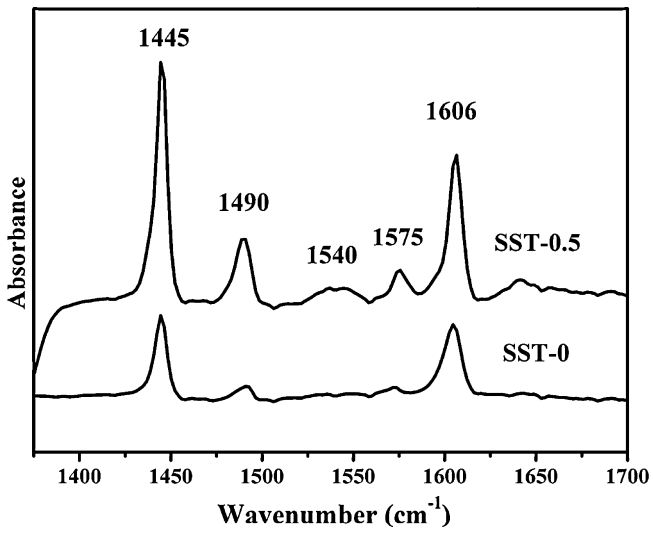

Fig. 4. FTIR-pyridine thermodesorption spectra of the S-doped and sulfate TiO_2.

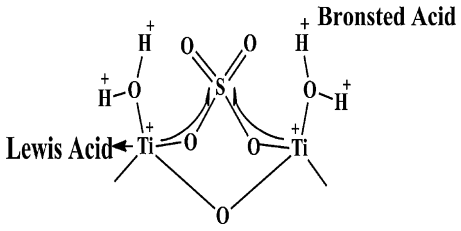

Scheme 1. Schematic representation of the Brönsted and Lewis acid sites present in the S-doped and sulfate TiO_2.

which shows that the S-doped and sulfate TiO_2 photocatalysts have stronger adsorption of H_2O.

3.4. X-ray photoelectron spectra (XPS)

To investigate the electronic environment and oxidation state of S in SST catalysts, XPS analysis has been performed. The XPS spectra of S-doped TiO_2 samples are shown in Fig. 5a. S 2p binding energy (BE) around 168.4 eV in the SST-0.5 catalyst can be divided into two isolated peaks at the binding energies of 167.5 and 168.8 eV, corresponding to chemical states of S^{4+} and S^{6+}, respectively [39]. The peak located at 167.5 eV indicates the presence of the Ti—O—S bond in the TiO_2 lattice, while another peak at 168.8 eV shows that SO_4^{2-} ions are anchored on the surface of TiO_2 [37]. Fig. 5b shows the binding energies of the spin-orbit components ($2p_{3/2}$ and $2p_{1/2}$) of Ti 2p observed to be at 458.1 and 463.7 eV, respectively, which should be assigned to Ti^{4+} of TiO_2 (corresponding to Ti^{4+} in a tetragonal structure) [40]. There is a little positive shift of binding energy of Ti 2p by 0.3 eV, which may be caused by the bridged bidentate structure between SO_4^{2-} and Ti [36]. Meanwhile, a great difference is shown in Fig. 5 with the sulfur doping and sulfation of TiO_2. For the SST-0 catalyst (Fig. 5c), the O 1s peak contains two dominant peaks at about 529.5 and 532.3 eV. The lower energy peak is due to Ti—O bonding in TiO_2 and the higher energy peak may be attributed to the O—H bonds on the surface [41]. The high resolution spectrum of O 1s peaks of the SST-0.5 is shown in Fig. 5d. Curve-fitting result suggests that four kinds of oxygen exist in S-doped and sulfate TiO_2. The peaks at around 529.5 and 530.3 eV, can be attributed to the oxygen in Ti—O—Ti, Ti—O—S in the TiO_2 crystal lattice, and the peaks at 531.3 and 532.7 eV may be associated with O in sulfate [21] and surface O—H, respectively. The sulfur doping and sulfation of

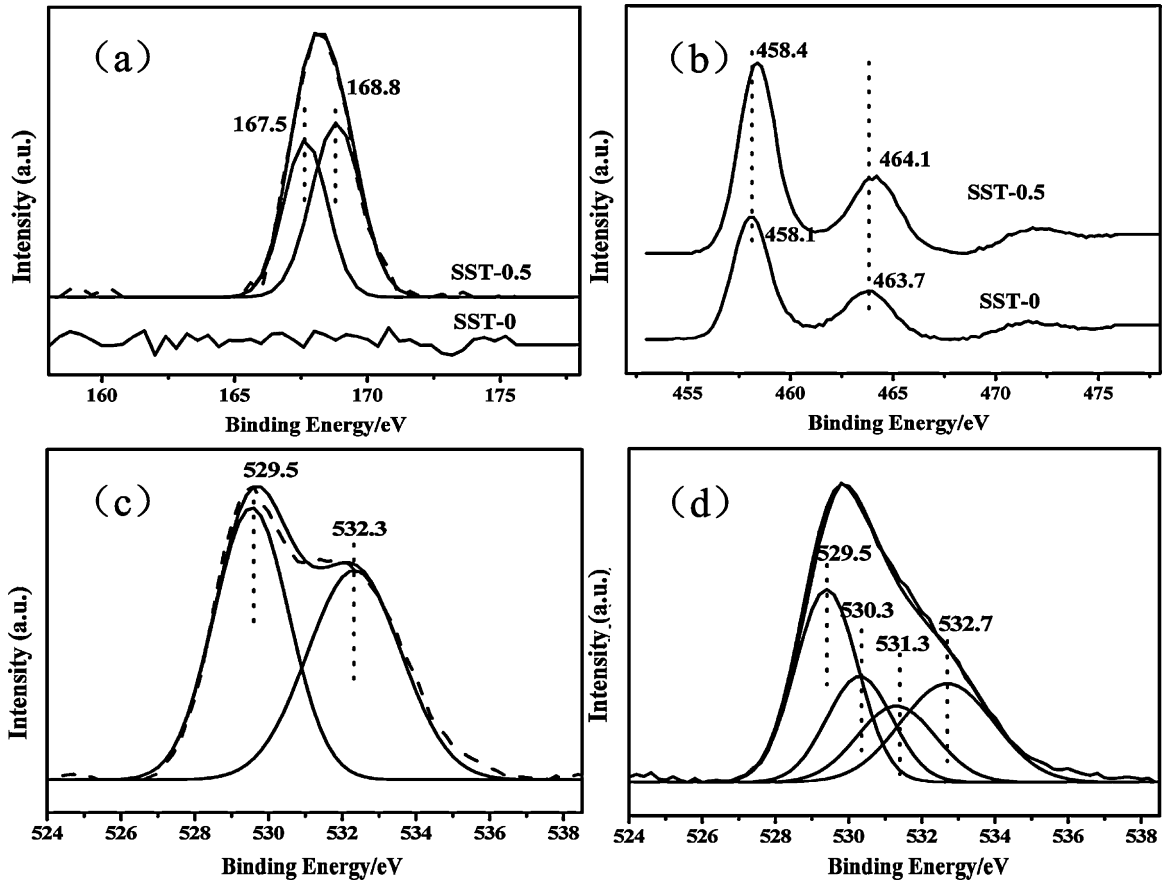

Fig. 5. The XPS spectra of the S-doped and sulfate TiO_2 catalysts. S 2p (a), Ti 2p (b), O 1s of SST-0 (c), O 1s of SST-0.5 (d).

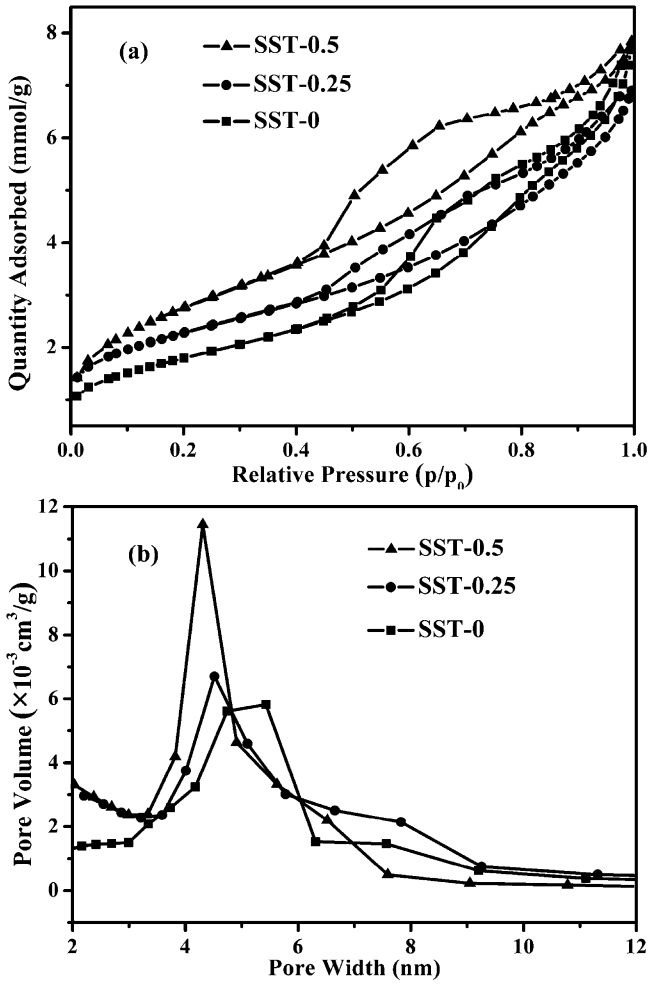

Fig. 6. N_2 adsorption–desorption isotherms of S-doped and sulfate TiO_2 catalysts (a), and pore size distribution (b).

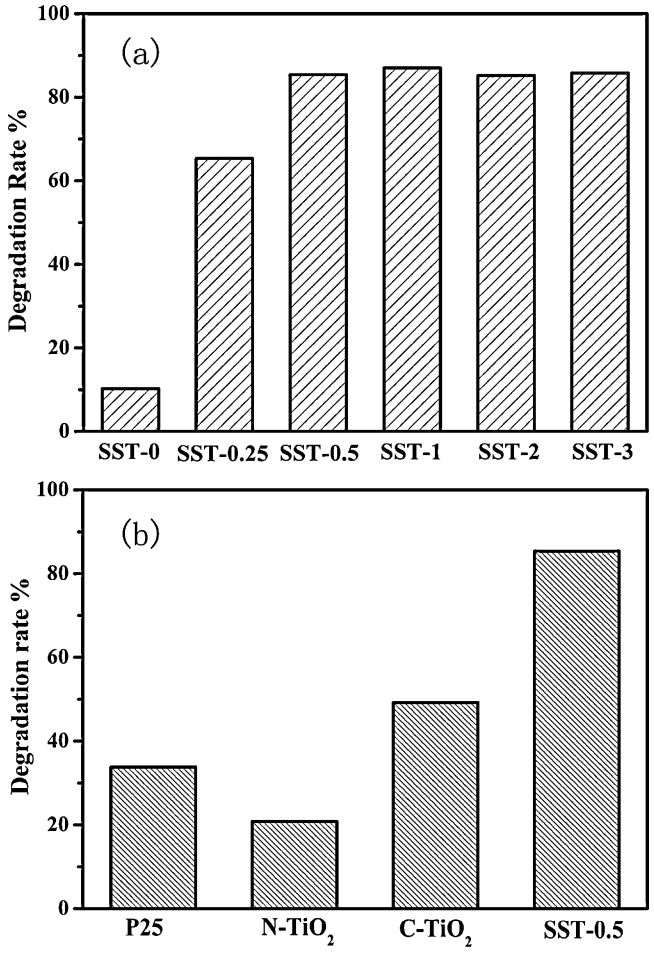

Fig. 7. The phenol degradation of S-doped TiO_2 catalysts under visible light for 10 h (a), the photocatalytic activity of P25, N-TiO_2, C-TiO_2 and SST-0.5 catalysts (b).

TiO_2 results in the change of chemical properties, leading to many differences between undoped and S-doped TiO_2 depicted by XPS results, as well as FTIR.

3.5. BET-surface areas

Fig. 6a shows the N_2 adsorption–desorption isotherms of SST catalysts. The samples show a type-IV isotherm with an H_3 type hysteresis loop [41], which can be ascribed to the larger secondary mesopores. It should be mentioned that the pore size distribution of SST-0.5 is regular compared with that of SST-0 and SST-0.25, which is shown in Fig. 6b. The pore size distribution measurement indicates that the SST-0.5 catalyst has a pronounced mesoporosity with an average pore diameter about 4 nm. The distance between TiO_2 particles become smaller with sulfur increasing, which can enhance the effective utilization of charge carriers. The BET specific surface areas, pore volumes of TiO_2 samples were summarized in Table 2. Compared with undoped TiO_2, the particle size of the S-doped TiO_2 samples is much smaller, resulting in larger specific surface area. Small particle size can shorten the route for an electron migration from the interior of TiO_2 to surface, which can reduce the recombination of h^+ and e^-. Moreover, the larger the surface area, the more SO_4^{2-} it has. The SO_4^{2-} adsorbed on the surface of TiO_2 can trap photo-induced electrons (e^-), improving the quantum yield.

Table 2
Pore size and surface area of SST samples.

Samples	Pore size (nm)	Pore volume (cm^3/g)	Surface area (m^2/g)
SST-0	6.44	0.24	146.07
SST-0.25	4.81	0.22	183.45
SST-0.5	3.94	0.21	216.22

3.6. Photocatalytic degradations

Photodegradation of phenol was employed to evaluate the photocatalytic activities of S-doped and sulfated TiO_2 catalysts. Fig. 7a shows the degradation rate of phenol over undoped TiO_2 and S-doped TiO_2 under visible light irradiation for 10 h. With the increasing sulfur doping, the photocatalytic degradation rate of phenol increases first, then it reaches a maximum value. This may be as a result of the sulfur doping and sulfation of TiO_2 attaining saturation point as the amount of $K_2S_2O_8$ added is increased. The optimal mole ratio of $K_2S_2O_8$ to TBOT is 0.5. The degradation rate of phenol can be up to 85.4%. The phenol degradation of P25, N-TiO_2 and C-TiO_2 which have been reported shows in Fig. 7b, the SST-0.5 catalyst has much higher activity of phenol degradation. Therefore, the S-doped and sulfate TiO_2 catalysts prepared in present work have excellent activities for phenol degradation under visible light.

3.7. Mechanism of the phenol degradation

As is known, the wide band gap energy of TiO_2 limits the absorption to ultraviolet light ($\lambda < 387$ nm), resulting in the lower photocatalytic activity of TiO_2 under visible light irradiation. However, the S-doped TiO_2 catalysts show high degradation rate

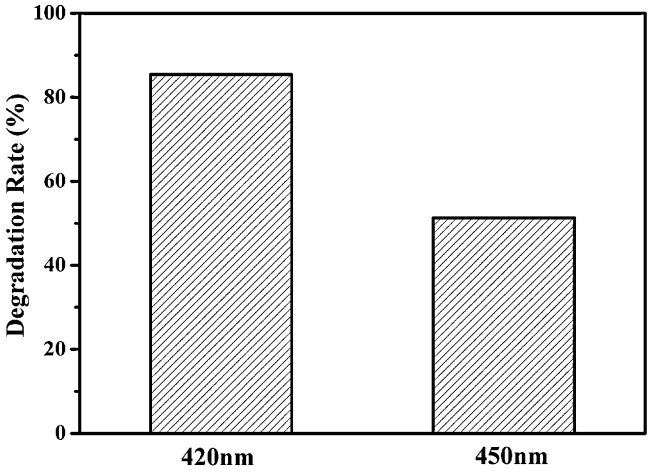

Fig. 8. The photoactivity of SST-0.5 for phenol photocatalytic degradation under different wavelength irradiation.

of phenol under visible light irradiation. They also exhibit high degradation activity when we use longer visible light ($\lambda > 450$ nm) irradiation as shown in Fig. 8. The phenol degradation rate of SST-0.5 catalyst is 51.3% under longer visible light irradiation for 10 h, which demonstrates the S-doped and sulfate TiO_2 has an excellent utilization in the longer visible light region.

In order to further explore the mechanism of the phenol degradation, we tried to remove the surface SO_4^{2-} adsorbed on the S-doped TiO_2 photocatalysts by washing them with NaOH (0.1 M). The FTIR spectra and the activity results are shown in Fig. 9. FTIR spectra demonstrate that the surface SO_4^{2-} of the SST-0.5 photocatalyst is washed off completely. However, the activity of it only decreased to 47.2%, which is higher than that of undoped TiO_2 and lower than that of S-doped and sulfated TiO_2. It is known that the PL emission is the result of the recombination of excited electrons and holes, the lower PL intensity may indicate the lower recombination rate of electron–holes under light irradiation. The PL spectra of the SST-0.5 samples before and after washing with sodium hydroxide are shown in Fig. 10. The PL emission intensity of SST-0.5 is lower than the one washed by 0.1 M NaOH, which indicates the decrease of recombination of electron and hole. From the SST-0.5 FTIR spectra (Fig. 9), it shows that the peaks of SO_4^{2-} disappear with washing the sample by 0.1 M NaOH. So it is found that the lower PL intensity may be caused by sulfate ions trapping photo-induced electrons, promoting the separation of electrons and holes.

Therefore, the results show that the high activity of the S-doped and sulfate TiO_2 photocatalysts resulted from the synergistic effect between S^{4+} doped into the crystal lattice and SO_4^{2-} anchored on the surface. The detailed process of charge transfer is described in Scheme 1. Zheng et al. [42] have reported the band gap energy of cation S as 2.61 eV by the density functional theory (DFT) calculation. We have calculated the band gap energy of S-doped and sulfate TiO_2 photocatalysts and it is 2.78–2.85 eV, so S-doped and sulfate TiO_2 photocatalyst can form an impurity energy level near the conduction band of TiO_2. The process of photo-induced electrons and holes producing and transferring is displayed in Scheme 2. With this impurity energy level, the photocatalysts can produce more photo-induced electrons (e^-) and photo-induced holes (h^+) under visible light irradiation. The electrons (e^-) can be injected from O 2p to the impurity energy level (S^{4+}), and transmitted to S^{6+} (SO_4^{2-}) on the surface of TiO_2. Then e^- can be transferred to O_2. The holes (h^+) can also move to the surface of the particle. Both photo-induced e^- and h^+ can produce hydroxyl radical ($OH^\bullet$), and the process of producing $OH^\bullet$ is as follows:

$$SST + h\nu \rightarrow SST + e^- + h^+ \quad (2)$$

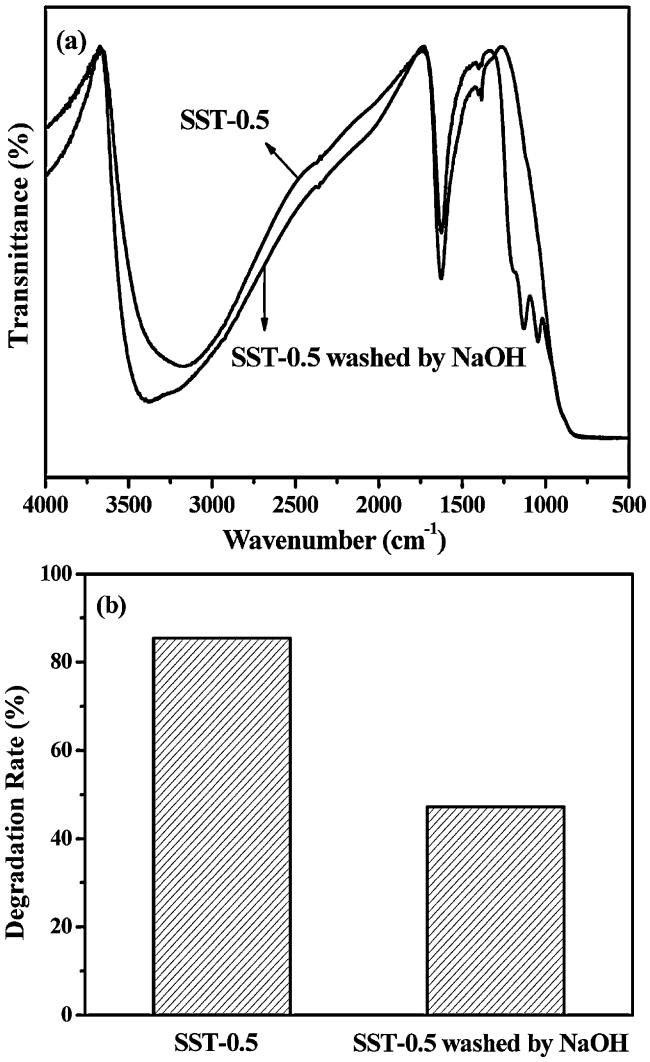

Fig. 9. The difference of SST-0.5 before and after washing. FTIR (a), photocatalytic activity (b).

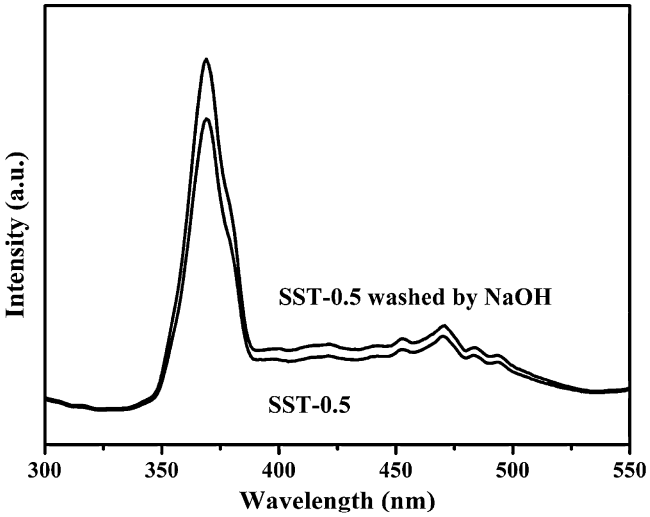

Fig. 10. The PL spectra of the SST-0.5 samples before and after washing with sodium hydroxide.

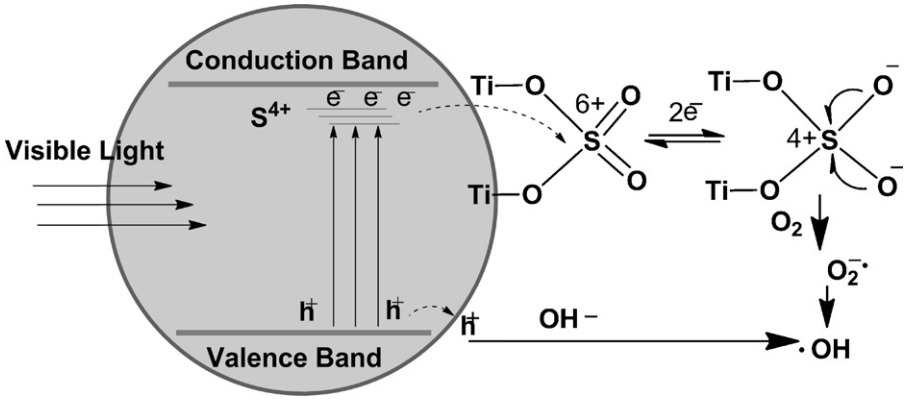

Scheme 2. The process of charge transfer for degradation of phenol.

$$OH^- + h^+ \rightarrow OH^\bullet \quad (3)$$

$$O_2 + e^- \rightarrow O_2^{\bullet -} \quad (4)$$

$$O_2^{\bullet -} + H^+ \rightarrow HO_2^\bullet \quad (5)$$

$$2HO_2^\bullet \rightarrow H_2O_2 + O_2 \quad (6)$$

$$H_2O_2 + e^- \rightarrow OH^\bullet + OH^- \quad (7)$$

Many groups [43,44] have reported the pathway of phenol degradation using TiO_2 as a photocatalyst. The degradation proceeds through the stepwise hydroxylated reaction, forming intermediates such as catechol (CC), hydroquinone (HQ), hydroxyhydroquinone (HHQ) and so on. The aromatic intermediates undergo further photocatalytic oxidation to ring cleavage to yield carboxylic acids and aldehydes, which can go to CO_2 and H_2O due to decorboxylation at last. Thus, the photocatalytic decomposition of phenol mainly occurs via hydroxylated compounds.

The high photocatalytic activity of the S-doped and sulfate TiO_2 may be ascribed to two factors. A shift of the absorption edge toward the visible light regions of the solar spectrum is observed for S-doped and sulfate TiO_2 and there is a decrease in the band gap of S-doped TiO_2 nanoparticles with increase in S doping. The lower band gap width can be irradiated by light with longer wavelength (visible light), producing more excited electrons (e^-) and holes (h^+), which can improve the photoactivity. Moreover, the S-doped and sulfate TiO_2 catalysts have small particle sizes and large specific surface area as shown in the XRD and BET spectra, which reduces the path length for charge carriers diffused from the bulk to the surface of TiO_2, lessening the volume recombination probability of the charge carriers. On the other hand, SO_4^{2-} ions anchored on the surface of TiO_2 have strong affinity for electrons, capturing the photo-induced electrons (e^-), which hinders the recombination of electrons (e^-) and holes (h^+). In brief, the excellent photocatalytic activity of the S-doped and sulfate TiO_2 photocatalysts is caused by the cooperation effect between S^{4+} doped into the TiO_2 lattice and SO_4^{2-} anchored on the surface.

4. Conclusions

In summary, the S-doped and sulfate TiO_2 photocatalysts were prepared through a low-temperature solvothermal method using potassium persulfate as sulfur source. They show high photocatalytic activity for phenol photocatalytic degradation, and the optimal doping molar ratio of $K_2S_2O_8$ to Ti for phenol degradation is 0.5 under visible light irradiation. The degradation rate of phenol can be up to 85.4% in 10 h. For the S-doped and sulfate TiO_2 photocatalysts, sulfur exists in two primary forms: S^{4+} (doped into the crystal lattice to form an impurity level) and S^{6+} (SO_4^{2-} adsorbed on the surface of TiO_2). The catalysts have small particle sizes, large surface areas, which show red-shift absorption in the visible light region. The high photocatalytic activity of phenol is mainly resulted from the synergistic effect of S^{4+} and SO_4^{2-}. The S^{4+} substituted for Ti can form an impurity level, improving the utilization of visible light. SO_4^{2-} anchored on the surface is favorable for trapping photo-induced electrons (e^-), which can produce more hydroxyl radicals by suppressing the recombination between electrons and holes.

Acknowledgements

This work has been supported by National Basic Research Program of China (973 Program, 2010CB732306), National Nature Science Foundation of China (21007016 and 20977030), the Project of International Cooperation of the Ministry of Science and Technology of China (2011DFA50530), Science and Technology Commission of Shanghai Municipality (10520709900 and 10JC1403900) and the Fundamental Research Funds for the Central Universities.

References

[1] A. Fujishima, K. Honda, Nature 238 (1972) 37–38.
[2] T. Umebayashi, T. Yamaki, H. Itoh, K. Asai, Appl. Phys. Lett. 81 (2002) 454–456.
[3] T. Ohno, T. Mitsui, M. Matsumura, Chem. Lett. 32 (2003) 364–365.
[4] T. Ohno, M. Akiyoshi, T. Umebayashi, K. Asai, T. Mitsui, M. Matsumura, Appl. Catal. A-Gen. 265 (2004) 115–121.
[5] H.X. Li, X.Y. Zhang, Y.N. Huo, J. Zhu, Environ. Sci. Technol. 41 (2007) 4410–4414.
[6] F.E. Oropeza, J. Harmer, R.G. Egdell, R.G. Palgrave, Phys. Chem. Chem. Phys. 12 (2010) 960–969.
[7] M. Xing, J. Zhang, F. Chen, J. Phys. Chem. C 113 (2009) 12848–12853.
[8] J. Zhong, F. Chen, J.L. Zhang, J. Phys. Chem. C 114 (2010) 933–939.
[9] L.J. Chen, T. Wang, F. Chen, J.L. Zhang, Chin. J. Catal. 32 (2011) 699–703.
[10] M.Y. Xing, W.K. Li, Y.M. Wu, J.L. Zhang, X.Q. Gong, J. Phys. Chem. C 115 (2011) 7858–7865.
[11] Y.M. Wu, M.Y. Xing, J.L. Zhang, F. Chen, Appl. Catal. B-Environ. 97 (2010) 182–189.
[12] X.N. Lu, B.Z. Tian, F. Chen, J.L. Zhang, Thin Solid Films 519 (2010) 111–116.
[13] X.T. Hong, Z.P. Wang, W.M. Cai, F. Lu, J. Zhang, Y.Z. Yang, N. Ma, Y.J. Liu, Chem. Mater. 17 (2005) 1548–1552.
[14] J.A. Navio, G. Colon, M. Macias, C. Real, M.I. Litter, Appl. Catal. A-Gen. 177 (1999) 111–120.
[15] C. Adan, A. Bahamonde, M. Fernandez-Garcia, A. Martinez-Arias, Appl. Catal. B-Environ. 72 (2007) 11–17.
[16] L. Lin, W. Lin, Y.X. Zhu, B.Y. Zhao, Y.C. Xie, Chem. Lett. 34 (2005) 284–285.
[17] J.C. Yu, J.G. Yu, W.K. Ho, Z.T. Jiang, L.Z. Zhang, Chem. Mater. 14 (2002) 3808–3816.
[18] D. Li, H. Haneda, N.K. Labhsetwar, S. Hishita, N. Ohashi, Chem. Phys. Lett. 401 (2005) 579–584.
[19] J. Yu, S. Liu, Z. Xiu, W. Yu, G. Feng, J. Alloys Compd. 471 (2009) L23–L25.
[20] V. Nadtochenko, N. Denisov, A. Gorenberg, Y. Kozlov, P. Chubukov, J.A. Rengifo, C. Pulgarin, J. Kiwi, Appl. Catal. B-Environ. 91 (2009) 460–469.
[21] G. Colon, M.C. Hidalgo, G. Munuera, I. Ferino, M.G. Cutrufello, J.A. Navio, Appl. Catal. B-Environ. 63 (2006) 45–59.
[22] Y.M. Liu, J.Z. Liu, Y.L. Lin, Y.F. Zhang, Y. Wei, Ceram. Int. 35 (2009) 3061–3065.
[23] L.K. Noda, R.M. Almeida, N.S. Gon alves, L.F.D. Probst, O. Sala, Catal. Today 85 (2003) 69–74.

[24] A. Corma, A. Martinez, C. Martinez, J. Catal. 149 (1994) 52–60.
[25] H. Yang, R. Lu, L. Wang, Mater. Lett. 57 (2003) 1190–1196.
[26] H.X. Li, G.S. Li, J. Zhu, Y. Wan, J. Mol. Catal. A-Chem. 226 (2005) 93–100.
[27] A. Nakajima, H. Obata, Y. Kameshima, K. Okada, Catal. Commun. 6 (2005) 716–720.
[28] T. Jin, T. Yamaguchi, K. Tanabe, J. Phys. Chem. 90 (1986) 4794–4796.
[29] M.Y. Xing, J.L. Zhang, F. Chen, J. Phys. Chem. C 113 (2009) 12848–12853.
[30] M.Y. Xing, D.Y. Qi, J.L. Zhang, F. Chen, Chem. Eur. J. 17 (2011) 11432–11436.
[31] P.P. Bidaye, D. Khushalani, J.B. Fernandes, Catal. Lett. 134 (2010) 169–174.
[32] H.Y. Liu, L. Gao, J. Am. Ceram. Soc. 87 (2004) 1582–1584.
[33] J.L. Ropero-Vega, A. Aldana-Perez, R. Gomez, M.E. Nino-Gomez, Appl. Catal. A-Gen. 379 (2010) 24–29.
[34] M. Dhananjeyan, E. Mielczarski, K. Thampi, P. Buffat, M. Bensimon, A. Kulik, J. Mielczarski, J. Kiwi, J. Phys. Chem. B 105 (2001) 12046–12055.
[35] T. Yamaguchi, Appl. Catal. 61 (1990) 1–25.
[36] X. Wang, J.C. Yu, Y. Hou, X. Fu, Adv. Mater. 17 (2005) 99–102.
[37] G. Colon, M.C. Hidalgo, J.A. Navio, A. Kubacka, M. Fernandez-Garcia, Appl. Catal. B-Environ. 90 (2009) 633–641.
[38] G. Colon, M.C. Hidalgo, J.A. Navio, Appl. Catal. B-Environ. 45 (2003) 39–50.
[39] P. Xu, T. Xu, J. Lu, S. Gao, N.S. Hosmane, B. Huang, Y. Dai, Y. Wang, Energy Environ. Sci. 3 (2010) 1128–1134.
[40] Y.Y. Lv, Y. Ding, J.H. Zhou, W.M. Xiao, Y.Y. Feng, J. Am. Ceram. Soc. 92 (2009) 938–941.
[41] Y.W. Wang, Y. Huang, W.K. Ho, L.Z. Zhang, Z.G. Zou, S.C. Lee, J. Hazard. Mater. 169 (2009) 77–87.
[42] J.W. Zheng, A. Bhattcahrayya, P. Wu, Z. Chen, J. Highfield, Z.L. Dong, R. Xu, J. Phys. Chem. C 114 (2010) 7063–7069.
[43] Z.Q. He, L. Xie, J.J. Tu, S. Song, W.P. Liu, Z.W. Liu, J.Q. Fan, Q. Liu, J.M. Chen, J. Phys. Chem. C 114 (2010) 526–532.
[44] K. Nagaveni, G. Sivalingam, M.S. Hegde, G. Madras, Environ. Sci. Technol. 38 (2004) 1600–1604.